

Supplementary Information for

**“Tailoring the Many-Body Effects and Phase Configurations in Monolayer MSi_2X_4
($M=Mo, W$; $X=N, P, As, Sb$) for Wide-Range Bandgap Engineering”**

Ya Yang^{1,#}, Xin Wang^{2,#}, Li Sun³, Fanhao Jia⁴, Yurong Ruan^{3,*}, Tao Feng^{3,*}, Yabei Wu^{3,*}

¹College of Physics and Electronic Engineering & Key Laboratory of Microelectronics and Energy of Henan Province, Xinyang Normal University, Xinyang 464000, China

²School of Physical Science and Technology, Nantong University, Nantong, 226019, China

³Department of Materials Science and Engineering and Guangdong Provincial Key Lab for Computational Science and Materials Design, Southern University of Science and Technology, Shenzhen, Guangdong 518055, China

⁴Department of Physics, School of Sciences, Hangzhou Dianzi University, Hangzhou 310018, China

*Corresponding author: ruanyr@sustech.edu.cn; fengt@sustech.edu.cn;
wuyb3@sustech.edu.cn*

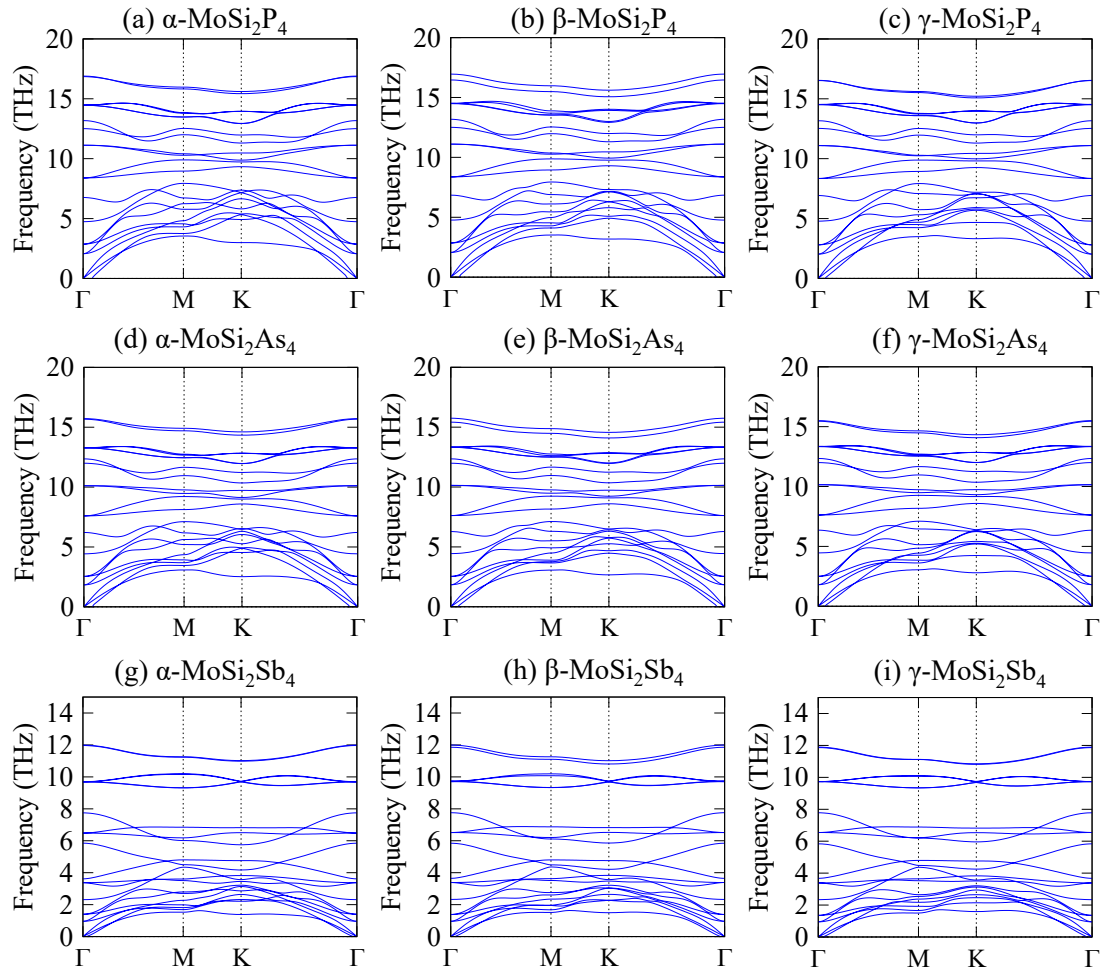


Fig. S1. Phonon spectra for the three different MoSi_2X_4 configurations ($X=\text{P}, \text{As}, \text{Sb}$).

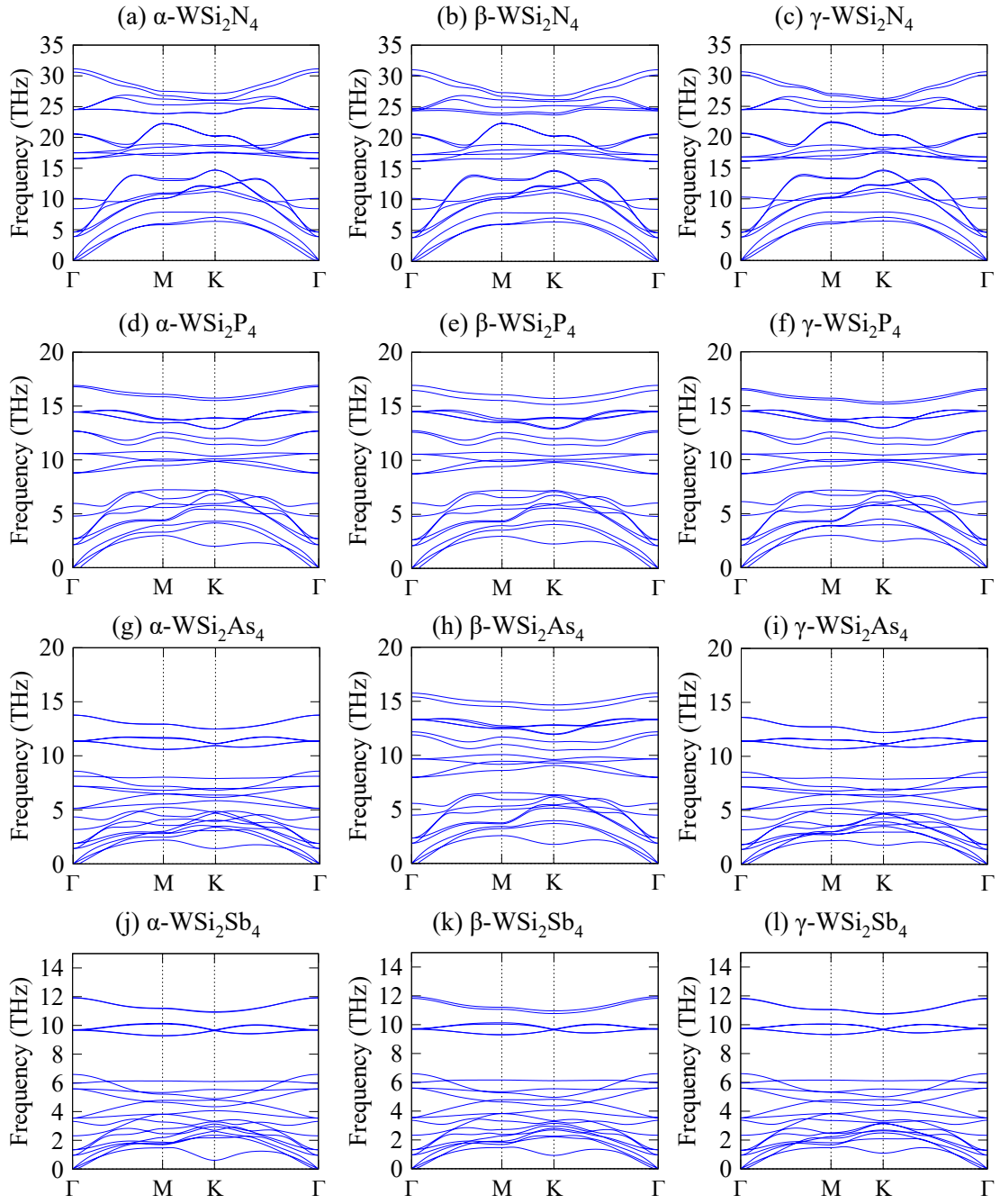


Fig. S2. Phonon spectra for the three different WSi_2X_4 configurations ($\text{X}=\text{N}, \text{P}, \text{As}, \text{Sb}$).

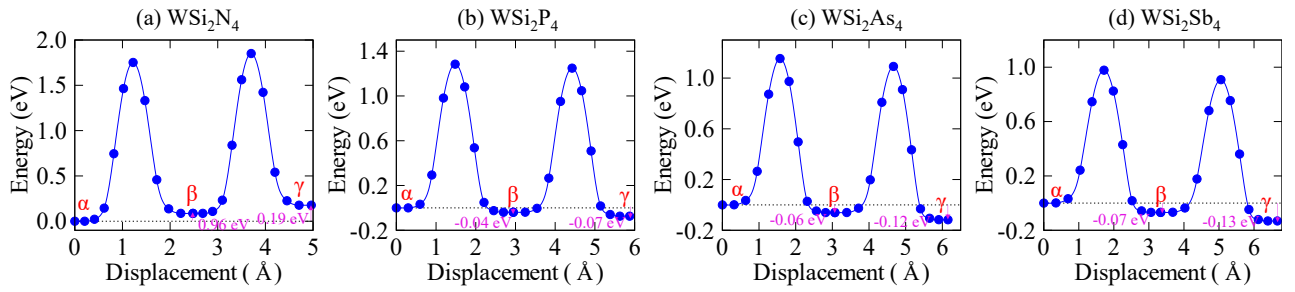


Fig. S3. Calculated energy barriers for the atomic migration path of X atoms in monolayer WSi_2X_4 (X=N, P, As, Sb).

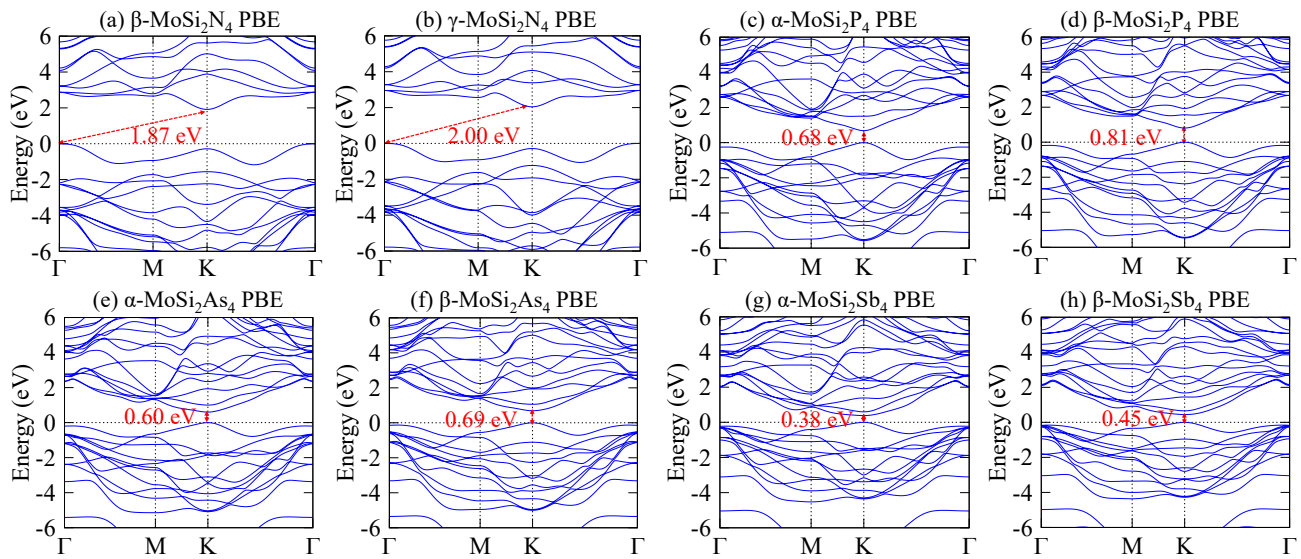


Fig. S4. DFT-PBE calculated band structures for the metastable monolayer MoSi_2X_4 configurations (X=N, P, As, Sb).

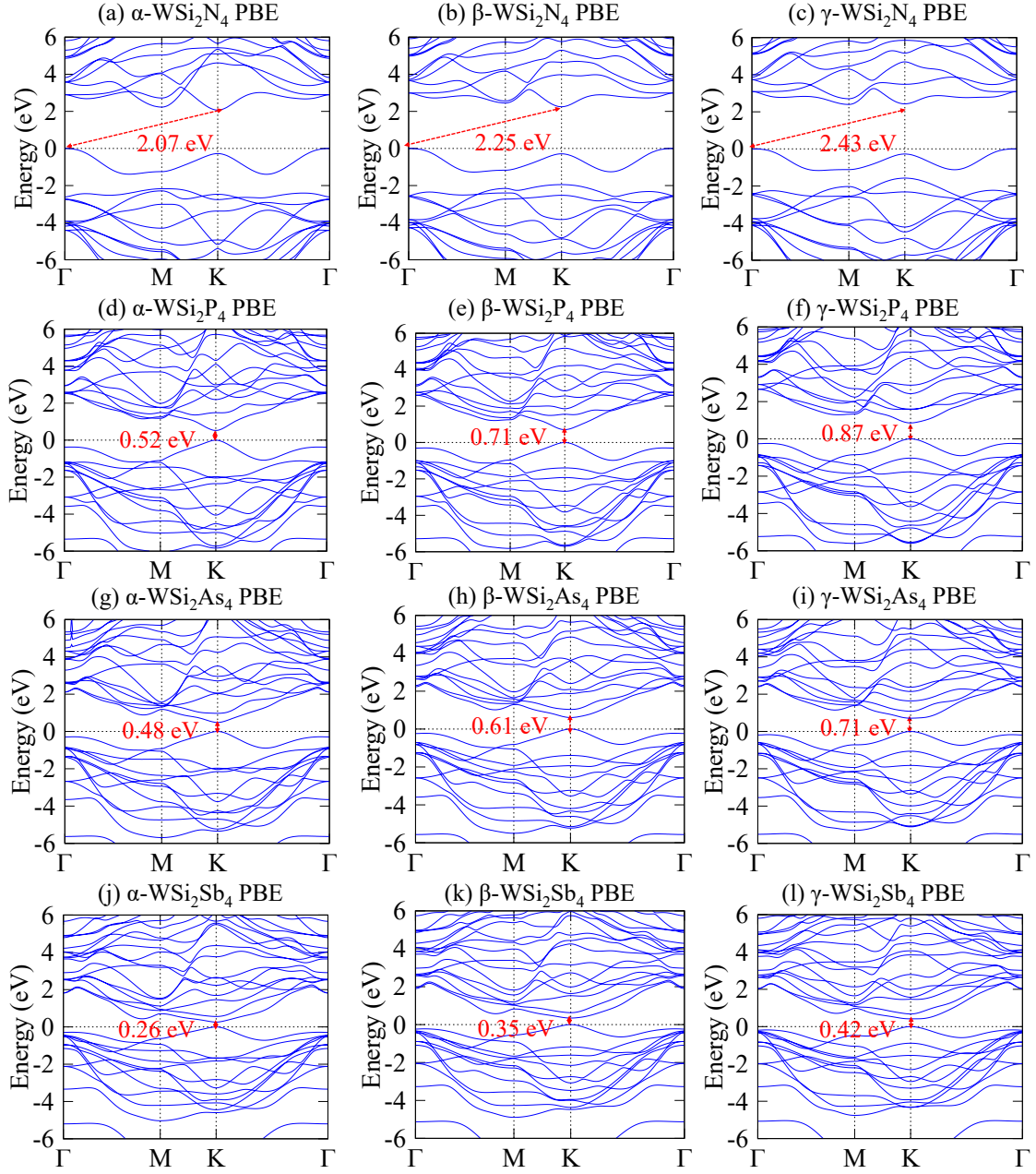


Fig. S5. DFT-PBE calculated band structures for all monolayer WSi_2X_4 configurations ($\text{X}=\text{N}, \text{P}, \text{As}, \text{Sb}$).

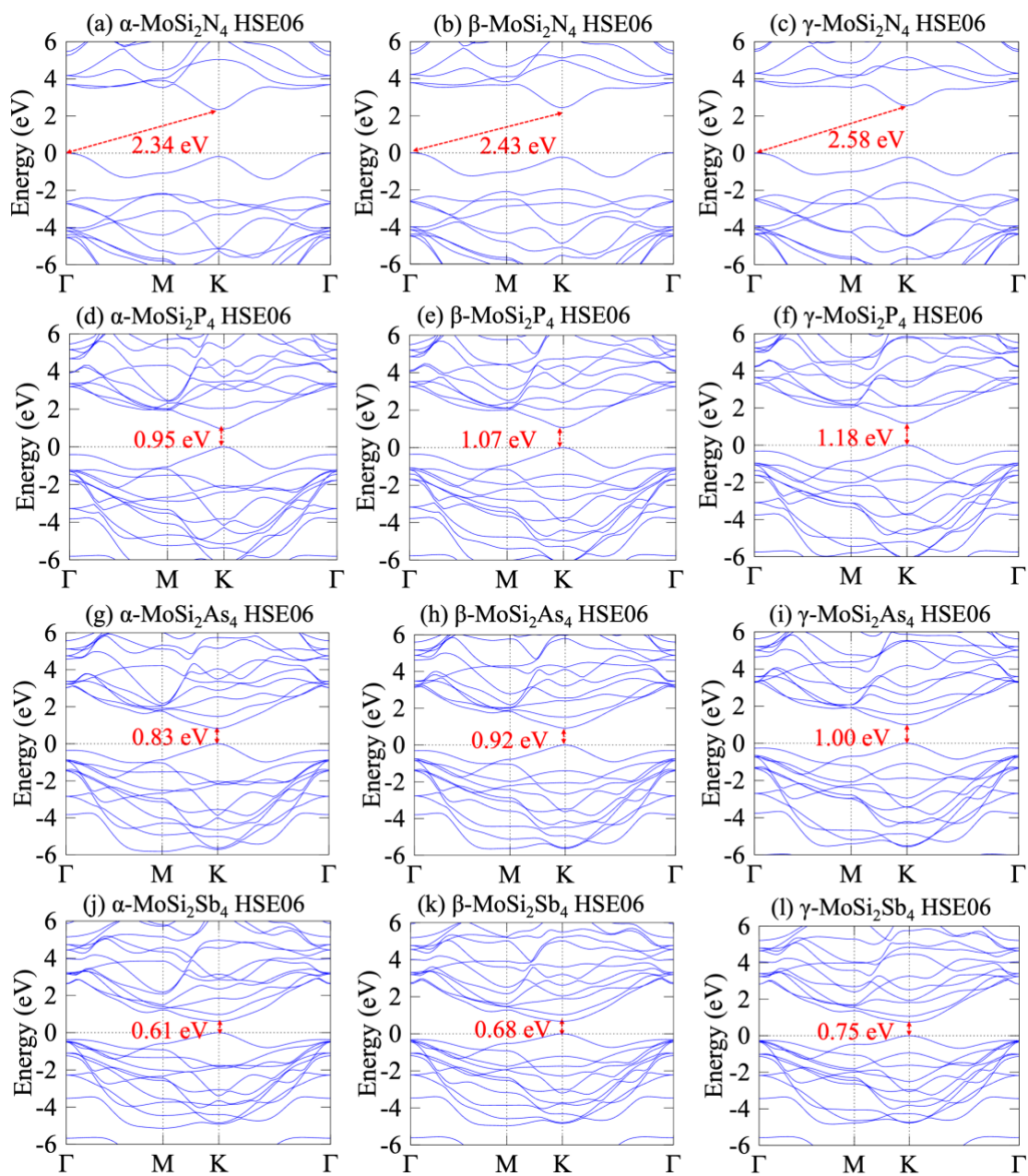


Fig. S6. DFT-HSE06 calculated band structures for all monolayer MoSi_2X_4 configurations ($\text{X}=\text{N}, \text{P}, \text{As}, \text{Sb}$).

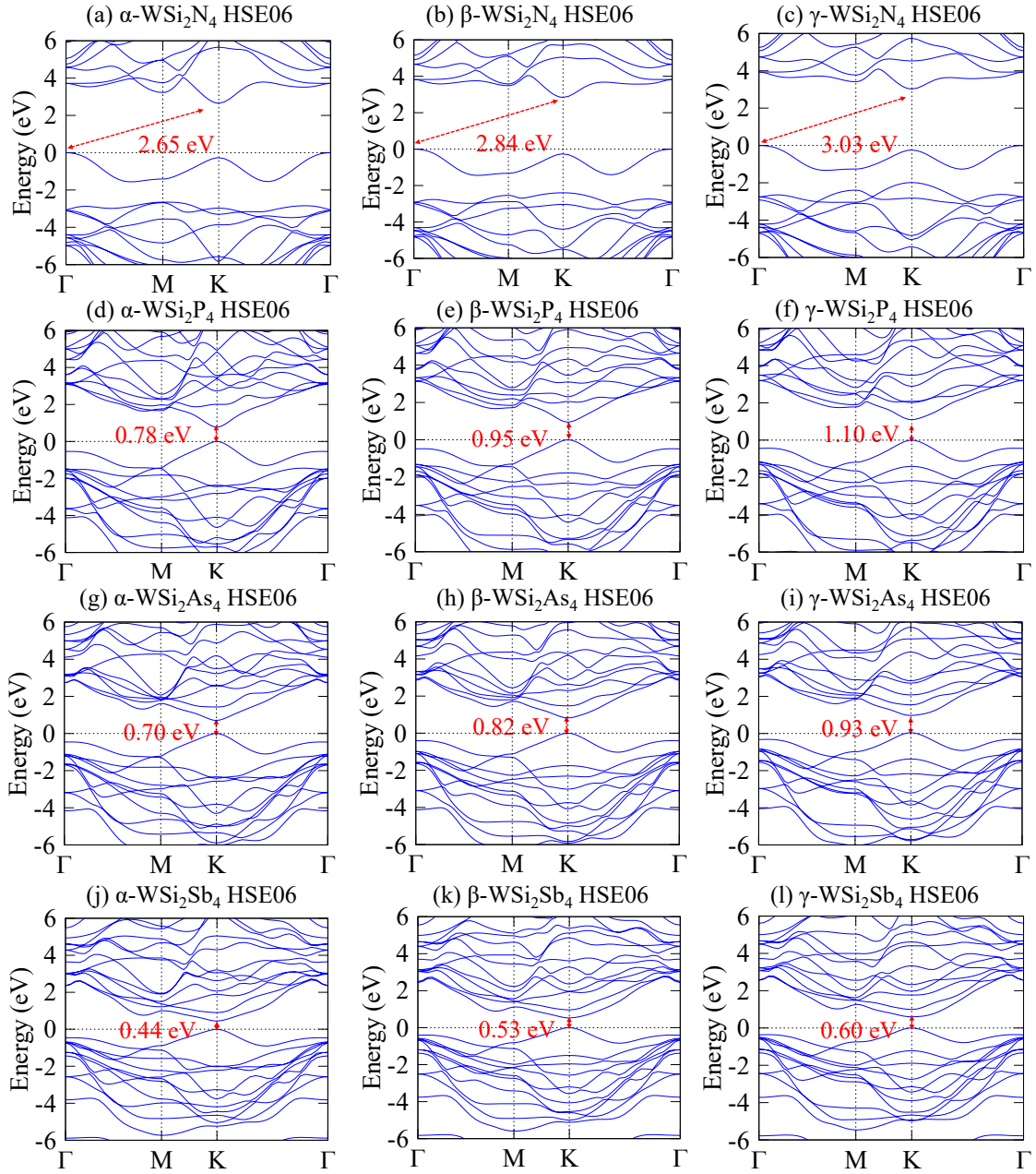


Fig. S7. DFT-HSE06 calculated band structures for all monolayer WSi_2X_4 configurations ($\text{X}=\text{N}, \text{P}, \text{As}, \text{Sb}$).

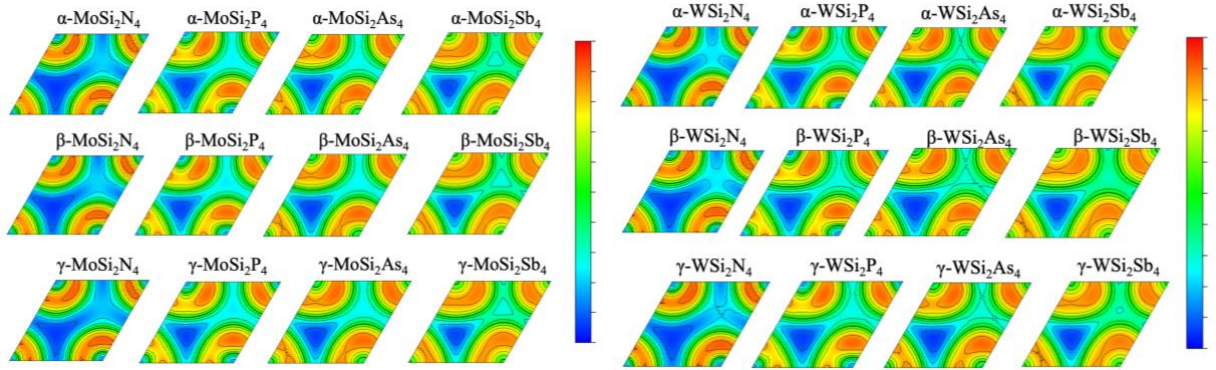


Fig. S8. Microscopic origin of the enhanced dielectric screening in MoSi_2X_4 (left panel) and WSi_2X_4 (right panel) ($\text{X}=\text{N}, \text{P}, \text{As}, \text{Sb}$) monolayers. 2D cross-sectional map of the Electron Localization Function (ELF) for the, taken along the plane containing the interior X atoms. The color bar represents the ELF magnitude from 0 (blue, fully depleted) to 1 (red, fully localized). This progressive delocalization of the p -orbitals from N to Sb directly visualizes the enhanced electronic polarizability, providing the microscopic basis for the increased macroscopic dielectric constant (ϵ_∞) and the dramatically reduced GW quasiparticle gap correction (ΔE_g) discussed in the main text.

Table S1. The band gaps (in eV) calculated by different methods (PBE, HSE06, GW) for the different configurations of monolayer MSi_2X_4 ($\text{M}=\text{Mo}, \text{W}$; $\text{X}=\text{N}, \text{P}, \text{As}, \text{Sb}$). The most stable configurations are marked in bold.

Phases	PBE			HSE06			GW		
	α	β	γ	α	β	γ	α	β	γ
MoSi_2N_4	1.79	1.87	2.00	2.34	2.43	2.58	2.82	2.88	3.02
MoSi_2P_4	0.68	0.81	0.91	0.95	1.07	1.18	1.21	1.27	1.35
MoSi_2As_4	0.60	0.69	0.76	0.83	0.92	1.00	1.04	1.09	1.15
MoSi_2Sb_4	0.38	0.45	0.50	0.61	0.68	0.75	0.68	0.75	0.76
Phases	PBE			HSE06			GW		
	α	β	γ	α	β	γ	α	β	γ
WSi_2N_4	2.07	2.25	2.43	2.65	2.84	3.03	3.19	3.31	3.50
WSi_2P_4	0.52	0.71	0.87	0.78	0.95	1.10	0.96	1.11	1.31
WSi_2As_4	0.48	0.61	0.71	0.70	0.82	0.93	0.89	0.91	1.07
WSi_2Sb_4	0.26	0.35	0.42	0.44	0.53	0.60	0.47	0.59	0.66

Supplementary Note 1

To further substantiate the reliability of this setup, particularly for the systems exhibiting unusually small quasiparticle corrections, we performed additional, explicit convergence tests for γ -WSi₂Sb₄. As shown in Supplementary Figure S9, we systematically tested convergence behavior with respect to the dielectric cutoff, the number of conduction bands, and the vacuum thickness (related to the lattice constant c). The results clearly demonstrate that a lattice constant of 30 Å, combined with our chosen cutoffs, safely converges the GW bandgap to within 0.02 eV.

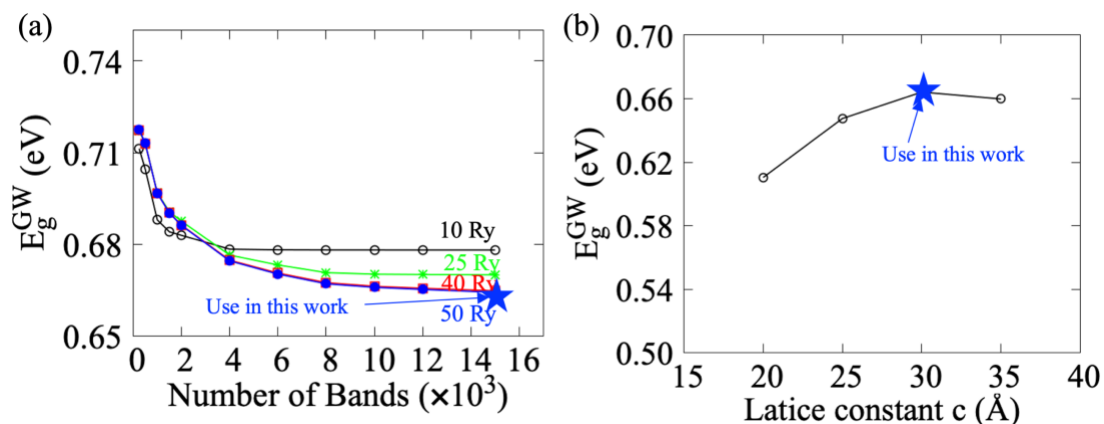


Fig S9. Convergence behavior of the calculated GW band gap for monolayer γ -WSi₂Sb₄ with respect to the kinetic energy cutoff for the dielectric matrices and the number of conduction bands included in the GW calculation (a) and the lattice constant c corresponding to the vacuum thickness (b).